What can be done with a good crystal and an accurate beamline?

Jiawei Wang,[a] Miroslawa
Dauter[a] and Zbigniew Dauter[b]*

[a]SAIC-Frederick Inc., Basic Research Program,
Argonne National Laboratory, Argonne,
IL 60439, USA, and [b]Synchrotron Radiation
Research Section, MCL, National Cancer
Institute, Argonne National Laboratory,
Argonne, IL 60439, USA

Correspondence e-mail: dauter@anl.gov

X-ray single-wavelength anomalous diffraction (SAD) data from a crystal of proteinase K were collected using synchrotron radiation of 0.98 Å wavelength at SER-CAT 22-ID beamline, Advanced Photon Source, Argonne National Laboratory. At this wavelength, the expected Bijvoet ratio resulting from the presence of one calcium, one chloride and ten S atoms in the 279-residue protein is extremely small at ~0.46%. The direct-methods program *SHELXD* located 11 anomalous sites using data truncated to 2 Å resolution. *SHELXE* was used to produce an easily interpretable electron-density map. This study shows that an accurate beamline and a good-quality crystal provide the possibility of successfully using a very weak anomalous signal of sulfur measured at a short wavelength for phasing a protein structure, even if a small degree of radiation damage is present.

1. Introduction

Anomalous scattering methods are currently widely used for phasing macromolecular structures. The multi-wavelength anomalous diffraction (MAD) technique (Hendrickson & Ogata, 1997) has become the most popular method for synchrotron radiation-based phasing of protein structures in the last decade (Hendrickson, 1999). In this approach, two or three data sets are usually collected at various wavelengths around the absorption edge of the anomalous scatterers present in the crystal. In the last few years, an experimentally simpler version of phasing, the single-wavelength anomalous diffraction (SAD) method, has gained popularity owing to its less demanding experimental requirements and to the availability of improved and more powerful phasing programs. Currently, the number of SAD structures exceeds the number of MAD-based depositions in the PDB (Minor *et al.*, 2006). The most popular vehicle for phasing based on anomalous signal is selenomethionine incorporated into recombinant proteins (Hendrickson *et al.*, 1990), but other anomalous atoms and ions that are inherently present (*e.g.* Fe, Zn, Cu in metalloproteins) or have been soaked into the crystal (heavy-atom reagents or halides) can also be utilized (Blundell & Johnson, 1976; Dauter *et al.*, 2000).

A search of non-redundant protein sequences in the NCBI database (http://www.ncbi.nlm.nih.gov/Database/) reveals that about 2.6% of the 3 952 980 protein sequences contain neither cysteine nor methionine residues, apart from the possible

N-terminal methionine. Therefore, the vast majority of proteins and all nucleic acids contain S or P atoms, respectively, which have considerable anomalous scattering contributions. The K absorption edge of sulfur lies in the very long wavelength region of X-ray radiation at 5.02 Å (Beardon & Burr, 1967), which practically precludes the use of the MAD approach. SAD is therefore the only choice for anomalous phasing based on sulfur. The first structure solved using the sulfur SAD (S-SAD) method was crambin (Hendrickson & Teeter, 1981), containing six S atoms in 45 amino acids, which at the wavelength of 1.54 Å provided a Bijvoet ratio $\langle \Delta F \rangle / \langle F \rangle$ of 1.5%. The classic work of Wang in the 1980s also advocated the possibility of sulfur SAD phasing (Wang, 1985). Since the late 1990s, many test proteins or novel structures have been studied by S-SAD phasing (see, for example, Table 1 in Ramagopal *et al.*, 2003). In all of these cases, in order to increase the anomalous signal from S atoms the wavelength was set to values longer than or equivalent to 1.54 Å and sometimes chromium radiation (λ = 2.29 Å) was used (Yang *et al.*, 2003; Kitago *et al.*, 2005; Watanabe *et al.*, 2005; Xu *et al.*, 2005; Watanabe, 2006). The disadvantage of increasing the wavelength is that another data set often has to be collected at the short wavelength if the high-resolution native data are needed for the ultimate refinement of the atomic model of the structure, since at long wavelengths high-resolution reflections may be not attainable owing to the increase in scattering angles.

Is it possible to collect only one data set for both S-SAD phasing and high-resolution structure refinement? In the present work, an attempt to phase a medium-size protein by S-SAD at a wavelength around 1 Å is presented in which the amount of anomalous signal is lower than 0.5%. The key points for successful phasing of the structure at such a short wavelength are the accuracy of the beamline and the quality of the crystal.

2. Crystallization and data collection

The serine proteinase from *Tritirachium album*, proteinase K, purchased from Sigma–Aldrich (catalogue No. P2308), was crystallized by the hanging-drop method. The protein solution (100 mg ml^{-1} in 50 mM HEPES buffer pH 7.0) was mixed in a 1:1 ratio with well solution consisting of 1 M NaNO$_3$ and 100 mM citrate buffer pH 6.5 (adjusted with HCl). Crystals appeared and grew within a few days. Using mother liquor supplemented with 30% glycerol as a cryoprotectant, a crystal of dimensions 0.4 × 0.4 × 0.3 mm was flash-cooled at 100 K in a stream of gaseous nitrogen. The crystal was set with its longest (c) axis almost parallel to the goniostat spindle axis, which helped to avoid the overlap of reflection profiles (Dauter, 1999), but no attempt was made to measure Bijvoet-related reflections on the same or even on neighbouring images. In this orientation, the appropriate 45° of rotation provides a complete data set for the crystal of class 422. X-ray data were collected to 1.27 Å resolution with a wavelength of 0.98 Å at the SER-CAT undulator beamline 22-ID, Advanced Photon Source (Argonne National Laboratory) using a MAR 300 CCD area detector. The beam intensity was attenuated to 10% to avoid saturation of the detector pixels. 330° of total rotation were measured with an exposure time of 2 s per image of 0.5° width. Data were processed using the *HKL*-2000 suite (Otwinowski & Minor, 1997), with the *hkl* and $-h-k-l$ reflections in an anomalous pair being treated as separate reflections during scaling and merging. To investigate the effect of the redundancy of measurements on the resulting accuracy of intensities, the collected diffraction images were processed in 11 sets of different redundancies, labeled 045, 060, 090, . . . , 330, using images corresponding to the first 45, 60, 90 . . . , 330° of the total crystal rotation. The data-collection statistics are summarized in Table 1. All calculations were performed with programs from the *CCP*4 suite (Collaborative Computational Project, Number 4, 1994), unless explicitly specified otherwise.

3. Anomalous signal in the data sets

Proteinase K contains one Ca and ten S (five Met and five Cys) atoms within 279 residues. According to the formula

Table 1
Data-collection statistics.

Values in parentheses are for the highest resolution shell.

(*a*) Overall statistics.

Protein	Proteinase K
Beamline	SER-CAT 22-ID
Unit-cell parameters (Å)	a = 67.55, c = 106.88
Space group	$P4_32_12$
Wavelength (Å)	0.98
Distance (mm)	150
Oscillation (°)/exposure time (s)	0.5/2
Transmission (%)	10
Mosaicity (°)	0.21
Resolution (Å)	50–1.27 (1.32–1.27)

(*b*) Statistics for data sets.

Data set	045	060	090	120	150	180	210	240	270	300	330
No. of images	90	120	180	240	300	360	420	480	540	600	660
Reflections measured	233747	312133	469031	625904	782977	939926	1096660	1253012	1410359	1567368	1723820
Unique reflections	62607	62979	63352	63503	63518	63529	63530	63532	63537	63537	63545
Completeness (%)	94.9 (88.5)	95.5 (89.9)	96.1 (91.3)	96.3 (91.2)	96.4 (92.5)	96.4 (92.6)	96.3 (91.6)	96.4 (92.7)	96.4 (92.7)	96.4 (92.7)	96.5 (92.7)
$I/\sigma(I)$	41.9 (10.7)	48.8 (12.8)	55.2 (16.9)	64.7 (20.0)	78.8 (23.0)	78.6 (24.1)	85.2 (25.3)	92.3 (28.1)	93.4 (28.3)	98.1 (29.8)	102.2 (30.1)
Redundancy	3.7 (3.7)	5.0 (4.9)	7.4 (7.2)	9.9 (9.6)	12.3 (12.0)	14.8 (14.3)	17.3 (16.7)	19.7 (19.1)	22.2 (21.5)	24.7 (23.9)	27.1 (26.3)
R_{merge} (%)	2.7 (11.0)	2.9 (11.4)	3.0 (11.8)	3.1 (11.9)	3.1 (12.1)	3.2 (12.1)	3.2 (12.3)	3.2 (12.4)	3.3 (12.5)	3.3 (12.8)	3.4 (13.1)
$R_{p.i.m.}$ (%)	1.7 (6.9)	1.4 (6.0)	1.2 (5.0)	1.0 (4.3)	0.9 (3.9)	0.9 (3.5)	0.8 (3.4)	0.7 (3.3)	0.6 (3.3)	0.6 (3.3)	0.6 (3.3)
B_{Wilson} (Å^2)	7.7	7.7	7.7	7.7	7.7	7.6	7.7	7.7	7.8	7.8	7.8

$\langle \Delta F^{\text{anom}} \rangle / \langle F \rangle = (2 \sum_i N_{Ai} f''^2_{Ai} / N_T)^{1/2} / Z_{\text{eff}}$ (Hendrickson & Teeter, 1981; Olczak *et al.*, 2003), where N_{Ai} and f''^2_{Ai} are the number and imaginary scattering contribution of anomalous scatterer of type i, N_T is the total number of non-H atoms in the molecule and Z_{eff} is the effective number of electrons of the 'average' protein atom (6.7), the expected Bijvoet ratio provided by one Ca atom, one Cl atom and ten S atoms contributing to the anomalous signal of this protein at 0.98 Å wavelength is ∼0.46%. Since a single measurement of an individual reflection intensity is generally burdened by errors of several percent, to achieve a sufficiently high accuracy for successful phasing with so weak an anomalous signal it is necessary to employ averaging multiple measurements of the same or symmetry-equivalent intensities. In the anomalous difference Patterson maps calculated with data sets of different redundancies, obvious peaks only appear after the total rotation reaches 150° or more. Fig. 1 shows graphs of various indicators of the anomalous signal over the whole range of data resolution (Dauter, 2006). Fig. 1(*a*) shows that as the redundancy increases, the estimated Bijvoet ratio diminishes but becomes closer to the level expected from the crystal content. According to the Hendrickson formula, the expected Bijvoet ratio (for zero diffraction angle) is 0.46%. In Fig. 1(*a*) the values calculated according to the modified formula, which takes into account the resolution-dependence of atomic form factors (Dauter *et al.*, 2002), are included and they agree well with the Bijvoet ratios calculated on the basis of the refined atomic model.

Other indicators, such as χ^2, R_{merge} and measurability, display only marginal amounts of anomalous signal in the data. However, as evidenced in Fig. 2(*a*), the peak heights in the anomalous difference Fourier map also increase gradually. The anomalous difference Fourier map for the most accurate data set 330 is shown in Fig. 2(*b*).

4. Substructure detection and phasing

4.1. Phasing with high-redundancy and high-resolution data

For the high-redundancy and high-resolution data 330, phasing proceeded very smoothly. The program *XPREP* (Sheldrick, 2001) was used to extract anomalous differences and the program *SHELXD* (Schneider & Sheldrick, 2002) was employed to locate the positions of anomalous scatterer sites, with the data resolution truncated to 2.0 Å, at which resolution the correlation coefficient between two partial subsets of
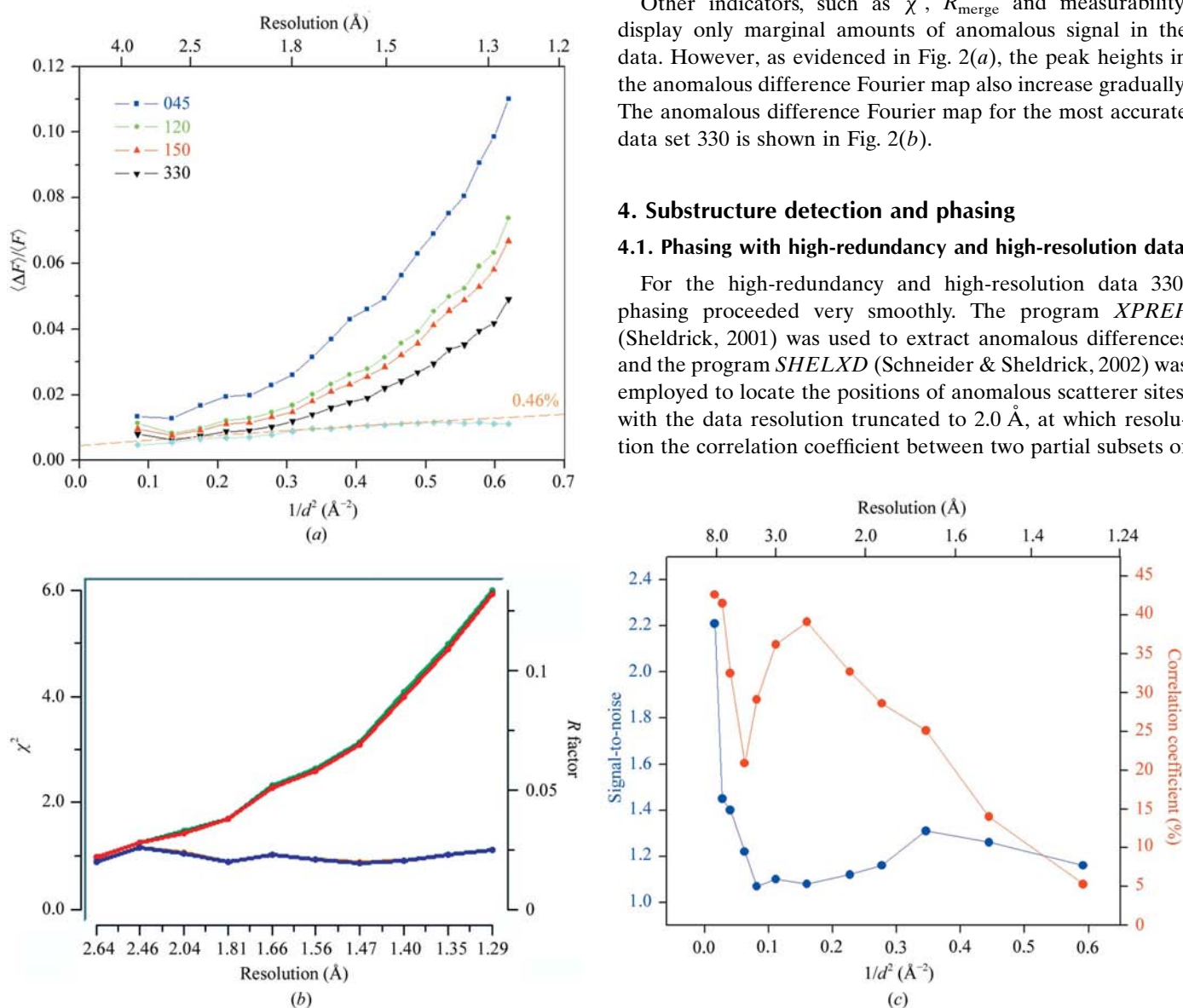
Figure 1
Anomalous signal indicators in resolution ranges. (*a*) The $\langle \Delta F^{\pm} \rangle / \langle F \rangle$ Bijvoet ratios for data of various redundancy. The cyan dots are calculated on the basis of the refined model and the orange line gives the theoretical estimation according to the modified Hendrickson formula (Dauter *et al.*, 2002). (*b*) R_{merge} and χ^2 values for data 330 (Otwinowski & Minor, 1997). (*c*) $\langle \Delta F^{\pm} \rangle / \langle \sigma(F) \rangle$ signal-to-noise (blue, left scale) and correlation coefficient between two separately merged parts of data set 330 (red, right scale) (Schneider & Sheldrick, 2002).

the same set diminishes to ~30%, as shown in Fig. 1(c). The sites are listed in Table 2. There is a clear contrast between the occupancy of the first (Ca) and second (S) sites and between the last correct sulfur site (No. 11) and the first spurious site (No. 12). The identified anomalous scattering sites were input to *SHELXE* (Sheldrick, 2002) for phase estimation and density modification. An easily interpretable electron-density map, illustrated in Fig. 3, was obtained. This map was submitted to the automatic model-building program *ARP/wARP* (Perrakis *et al.*, 1999) and 271 residues of the total of 279 protein amino acids were built by the iterative free-atom density-modification and model-building procedure. The average mean phase error between the *SHELXE* and the final refined phases was 27°. The correlation coefficient (CC) between the electron-density maps calculated with phases from *SHELXE* and the phases obtained from the final refined model was 88.4% for the main chain and 81.6% for side chains. The final model rebuilding was performed using *Coot* (Emsley & Cowtan, 2004) and the protein structure was refined anisotropically with *SHELXL* (Sheldrick & Schneider, 1997)
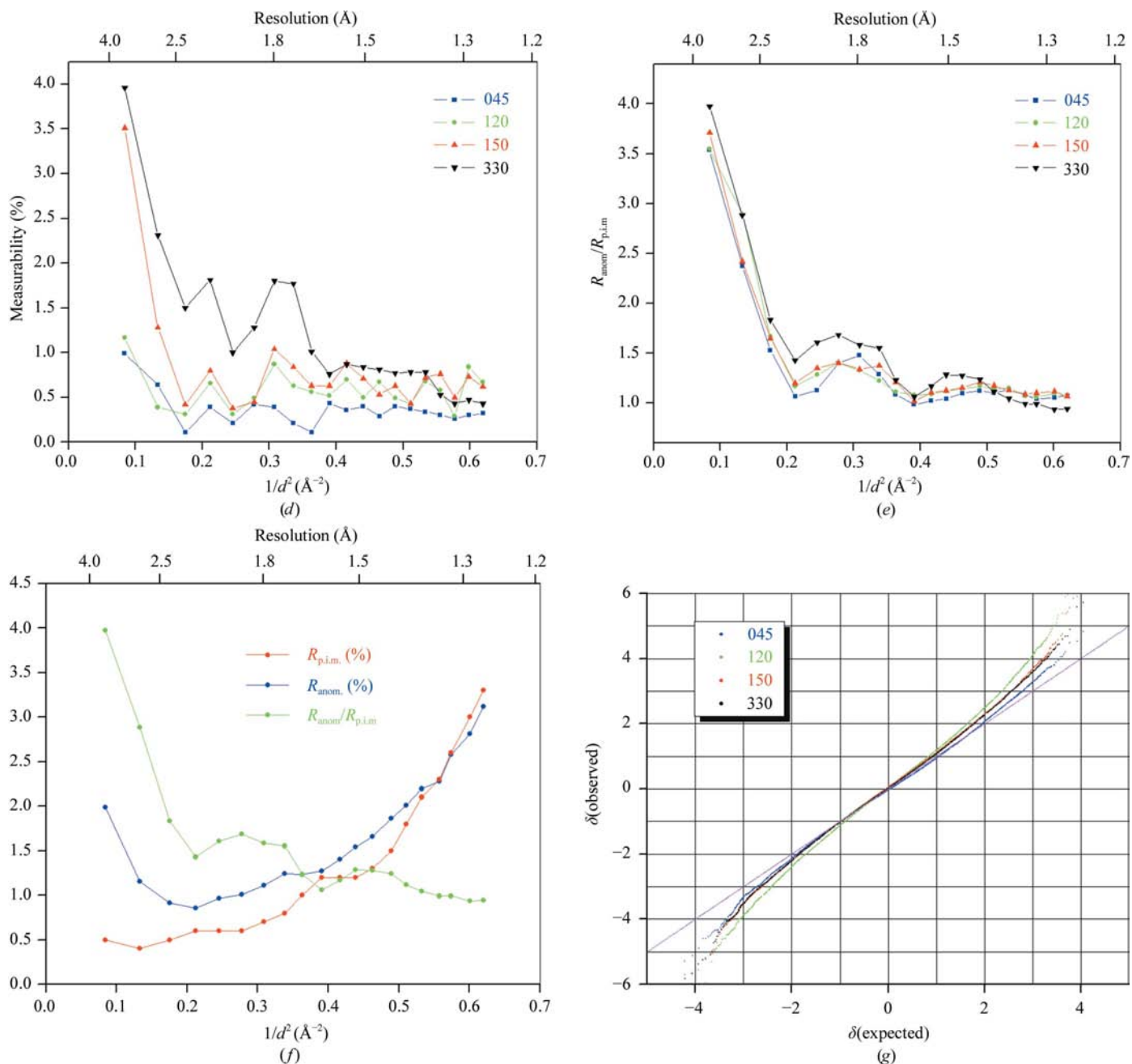

Figure 1 (continued)
(*d*) Measurability as a function of resolution (Zwart, 2005). (*e*) $R_{anom}/R_{p.i.m.}$ ratios (Mueller-Dieckmann *et al.*, 2005). (*f*) R_{anom}, $R_{p.i.m.}$ and their ratio for data 330. (*g*) Normal probability plot of anomalous differences $\delta_{anom} = (I^+ - I^-)/[\sigma^2(I^+) + \sigma^2(I^-)]^{1/2}$ (Howell & Smith, 1992).

Table 2
Sites located by *SHELXD* for data 330.

Rank	Site	Normalized occupancy
1	Ca	1.000
2	Cys73	0.510
3	Met111	0.497
4	Met225	0.457
5	Met55	0.456
6	Cys178	0.442
7	Met238	0.434
8	Cys123	0.394
9	Cys249	0.386
10	Met154	0.386
11	Cys34	0.370
12		0.140

Table 3
Difference between the positions of anomalous atoms in the refined model and those found by *SHELXD* or improved by anomalous difference Fourier map for data 120 in subsequent cycles of *SHELXE*.

Position	Cycle 1	Cycle 2	Cycle 3
Ca	0.067	0.056	0.043
SG_73	0.257	0.205	0.140
SD_111	0.435	0.356	0.259
SG_178	—	0.074	0.050
SD_55	—	0.135	0.105
SD_225	—	0.173	0.094
SD_238	—	0.132	0.076
SD_154	—	—	0.050
SG_123	—	—	0.049
SG_34	—	—	0.198
SG_249	—	—	0.091
Phase error (°)	65.17	54.71	32.92

to an R factor of 12.5% and an R_{free} of 15.9%, the latter based on a randomly selected 5% of the reflections.

The final model contains 279 protein residues, 251 water molecules, one calcium ion, one chloride ion, three nitrate anions and one molecule of boric acid inhibitor covalently bound to the catalytic Ser224 and to a molecule of glycerol.

The chloride ion was identified at the surface of the protein on the basis of its peak in the anomalous difference map. However, this site is partially occupied and the peak is much weaker than those corresponding to other anomalous scatterers (Fig. 2a). Judging from its peak height in the electron density and anomalous difference maps as well as its behaviour during refinement, the Cl$^-$ site is about 80% occupied. It was never located by *SHELXD*. A small amount of Cl$^-$ ions were present in the crystallization medium after adjusting the pH of the citrate buffer with hydrochloric acid. The unexpected boric acid derivative, covalently bound to the catalytic Ser224, was identified in the electron-density map (Fig. 4). Boric acid was not used in the preparation of the protein solution; it was present in the original sample of proteinase K. Evidently, it reacted with a molecule of glycerol used as a cryoprotectant. The whole moiety bound to Ser224 satisfactorily refined with full site occupancies for all atoms.

### 4.2. Phasing with high-resolution and low-redundancy data

For the high-redundancy data sets, 180, 210, ..., 330, *SHELXD* can identify all 11 anomalous sites and *SHELXE* can also phase the structure to the weighted mean phase error of about 23° (Fig. 5). With such a low mean phase error and 1.27 Å resolution, *ARP/wARP* could build almost all residues automatically in the corresponding electron-density map.

However, for data of lower redundancy the phasing procedure presented problems. With data sets 120 and 150 *SHELXD* could find only three and eight correct sites, respectively, among the 11 peaks asked for and output by the program. However, the iterative use of *SHELXE*, starting with the few located sites, led to the identification of all 11 sites in two (for data 150) or three (for data 120) iterations and to an interpretable map. The progress for data 120 is summarized in Table 3 and is illustrated in Fig. 6.
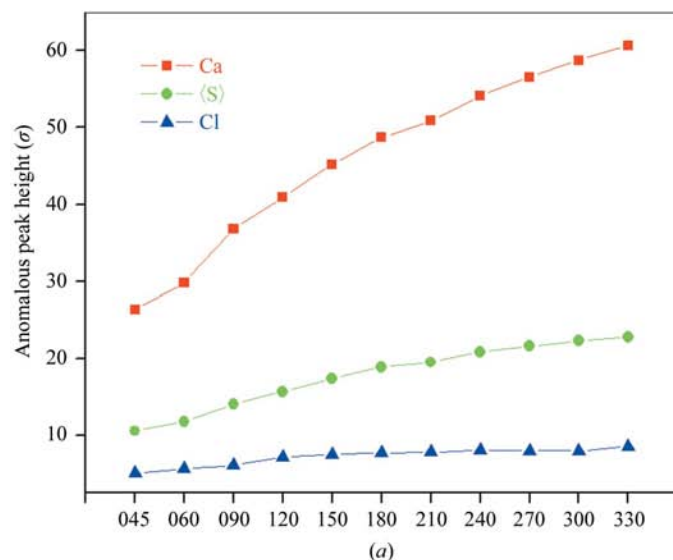
Figure 2
(a) The peak heights in the anomalous difference Fourier maps for data of various redundancies and (b) the anomalous difference Fourier map for data set 330 contoured at 4σ. The smallest peak in middle right of the figure is the Cl$^-$ ion and the peak furthest to the left is the Ca^{2+} ion.
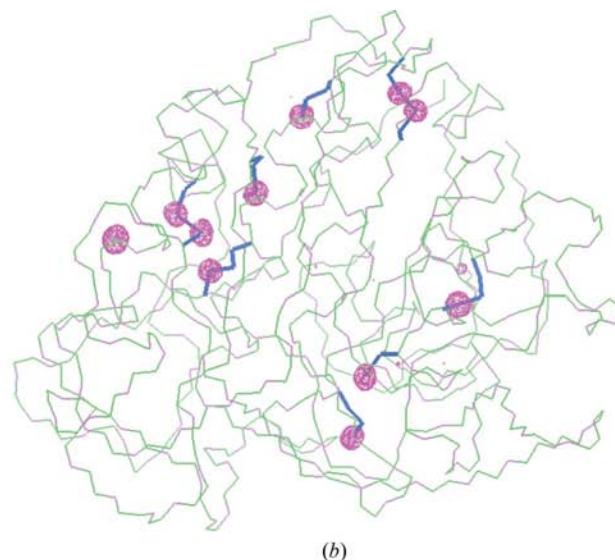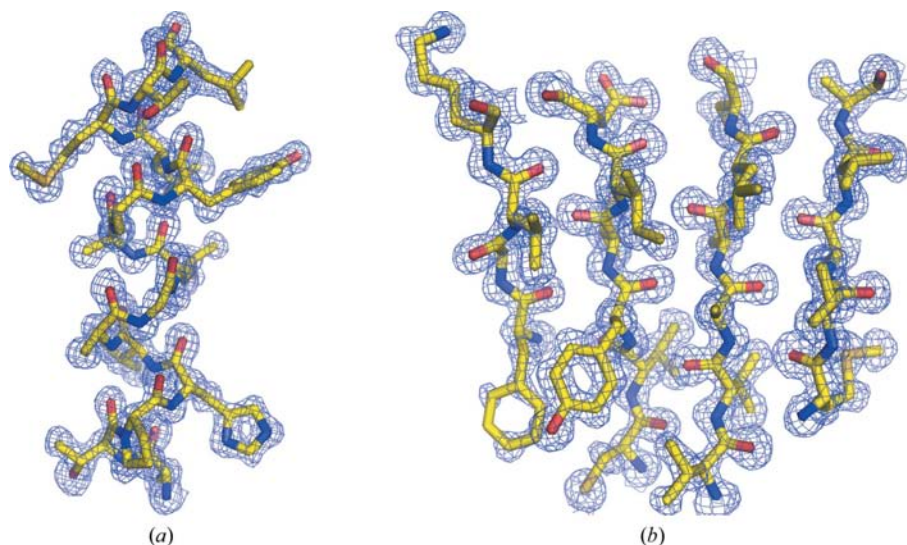
For data redundancy lower than 120°, *SHELXD* could not find any correct anomalous sites. If the known 11 sites found from data 120 were used for input to *SHELXE*, the anomalous signal in data 90 was still strong enough to produce a traceable electron-density map. Data 045 and 060 did not lead to any possibility of structure determination.

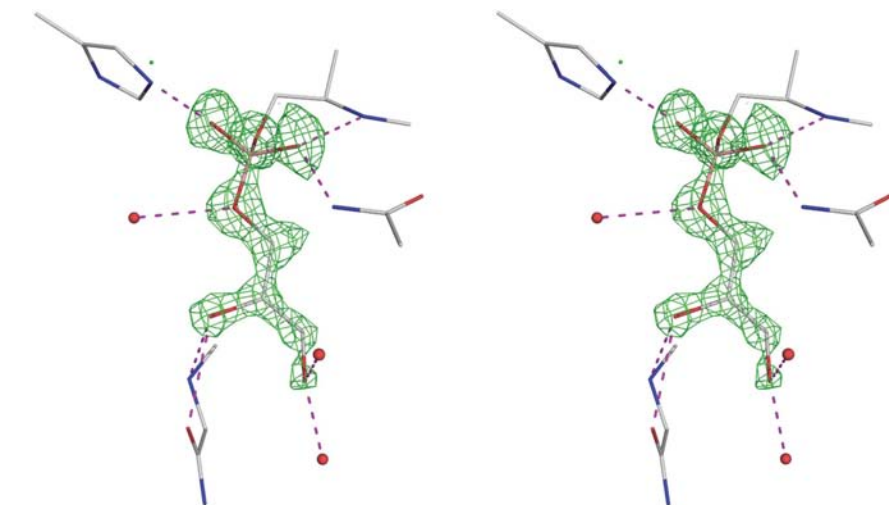### 4.3. Phasing with high-redundancy and low-resolution data

Data set 330 has the most accurately estimated anomalous signal of all the data sets. Even though the anomalous signal is very weak, the resolution reached 1.27 Å, which is beneficial for the density-modification procedure employed in

Figure 3
Electron-density maps contoured at 1σ after phasing and density modification by *SHELXE* for the 330 data. (*a*) The electron-density map of the α-helix (Ala226–Leu240); (*b*) the electron-density map of the β-sheet (Phe91–Lys94, Cys34–Asp39, Val127–Ser132, Met154–Ala158). Graphs were drawn with *PyMOL* (DeLano, 2002).
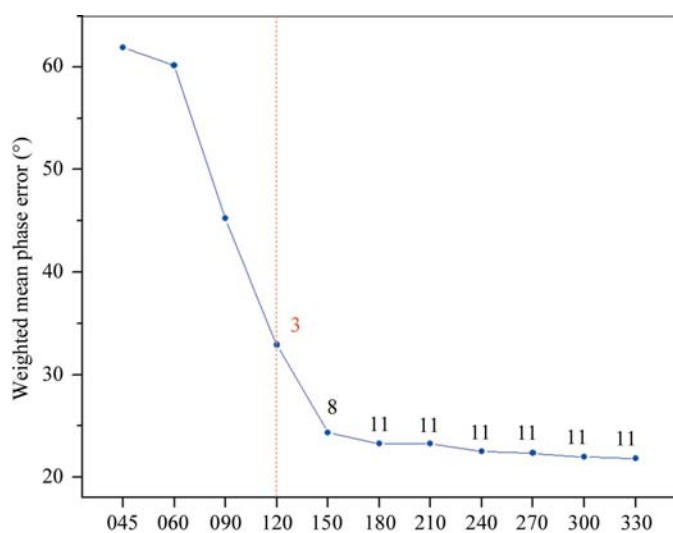

Figure 4
A stereo drawing of the OMIT map for the inhibitor bound to the catalytic Ser224. The map is contoured at 4σ. All hydrogen bonds involving the inhibitor are marked. The B atom is tetrahedrally coordinated by four O atoms forming covalent bonds with serine and glycerol.

SHELXE. To check the effect of data-resolution cutoff, the data 330 were truncated to different extents. When the resolution was truncated to 1.65 Å, *ARP/wARP* still built 274 residues in the map output by *SHELXE*. After cutting the resolution to 1.8 Å, *ARP/wARP* could not build any residues, but *RESOLVE* (Terwilliger, 2003*a*,*b*) built 103 residues. When the resolution limit was lower than 2 Å, *SHELXE* could not solve the structure. However, the use of the 2 Å data and the iterative dual-space fragment-extension algorithm in the program *OASIS*-2004 (Wang *et al.*, 2004) led to gradual improvement of phases, so that eventually *ARP/wARP* traced 274 residues automatically. *SHELXD* could still find all 11 sites when the resolution was truncated to 2.3 Å, but *RESOLVE* could build only 50 residues from the phases output by *OASIS*-2004. When the resolution was lower than 2.3 Å, the structure could not be solved by any of the above procedures. The results are summarized in Fig. 7, which shows the correlation coefficient between the maps obtained by *SHELXE* and *OASIS* with data truncated to different resolution and corresponding maps calculated with phases from the final refined model. The maps become uninterpretable when the map correlation coefficient drops below 50% and the corresponding average phase difference exceeds 60°.

4.4. Effect of radiation damage

In spite of the use of low exposures and X-ray beam attenuation in order to avoid overloaded pixels on the CCD detector, the crystal suffered some radiation damage. The total flux of the 10% attenuated X-ray beam passing through the collimator slits of dimensions 0.1×0.1 mm was 7×10^{10} photons s^{-1}. According to a calculation with *RADDOSE* (Murray *et al.*, 2004), the dose absorbed by the crystal during collection of 660 images was 3.3×10^6 Gy. This value is about six times smaller than the Henderson limit of 2×10^7 Gy (Henderson, 1990), *i.e.* the dose causing the total diffracted intensity to be halved. It may be noted that crystals of proteinase K are able to diffract to beyond 1.0 Å resolution (Betzel *et al.*, 2001); therefore, the data measured here, in spite of extending to 1.27 Å, can be treated as 'low resolution'. The B factors of individual images used in the data-scaling procedure did not exceed 0.88 Å^2. This means that intensities of

the highest resolution reflections (at 1.27 Å) in the last images were on average diminished to 88% in comparison with such reflections within the first images.

The Fourier map calculated with differences between amplitudes obtained from merging the first 45° and the last 45° of data and phases from the refined model revealed several sites showing the effects of radiation damage (Fig. 8). Two disulfide bridges were partially broken and a small number of acidic residues showed signs of decarboxylation. Interestingly, one of the three nitrate anions present in the model shows very clear signs of damage, whereas there are no features in the difference map at the sites of two other nitrate anions.

Figure 5
The weighted mean difference of phases obtained by *SHELXE* and those finally refined by *SHELXL* for data of various redundancies. The numbers at the points indicate the number of correct anomalous scatterer sites found by *SHELXD*. The dotted red line marks the limit of redundancy below which the structure could not be solved.
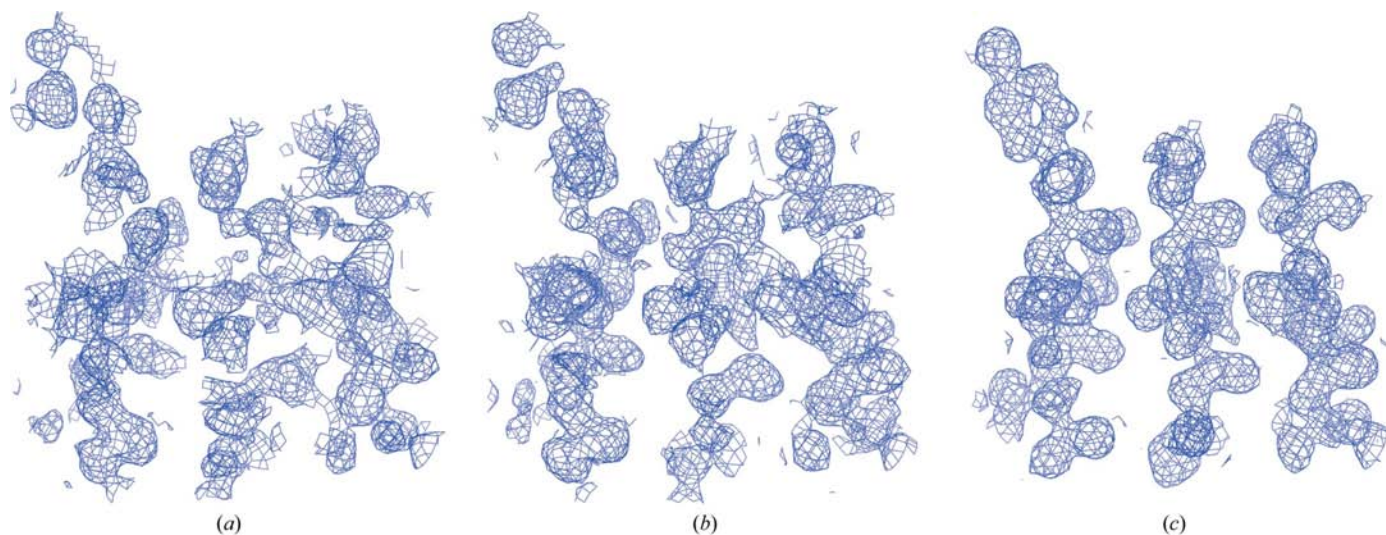
To estimate the effect of radiation damage more quantitatively, the R_d indicator (Diederichs, 2006) was calculated and is shown in Fig. 9. This is a merging R factor which depends on the difference between intensities of pairs of symmetry-equivalent reflections as a function of the difference between the images on which they appear, *i.e.* as a function of the difference between the X-ray dose absorbed by the crystal between recording these two reflections. The R_d curve is visibly modulated every 90°, which most probably results from the fact that during data collection fresh parts of the non-isometric crystal, which was larger than the beam, were exposed during data collection while it rotated around the spindle axis. However, the R_d curve displays an increasing tendency, confirming that the crystal was undergoing a degree of radiation damage. On average, the R_d value increased from 4.5 to 6.2% during the course of collecting all 660 diffraction images. The estimated rate of radiation damage, expressed as the srd parameter (Diederichs, 2006), is $5.4 \times 10^{-9}\,\mathrm{Gy^{-1}}$.

The extent of radiation damage suffered by the crystal of proteinase K is clearly identifiable in the statistics of the measured intensities as well as in the difference Fourier maps. However, this effect was evidently smaller than the level of the anomalous signal contained in the data and did not preclude the structure solution based on the very weak anomalous signal, despite the fact that no correction for radiation damage has been implemented during data reduction.

5. Conclusions

High-throughput crystallography requires a method by which the structures of native proteins can be determined quickly and easily. With this consideration, SAD phasing using intrinsic anomalous scatterers such as sulfur becomes increasingly attractive owing to advances in beamline hardware and phasing methods. The S-SAD data collected at the
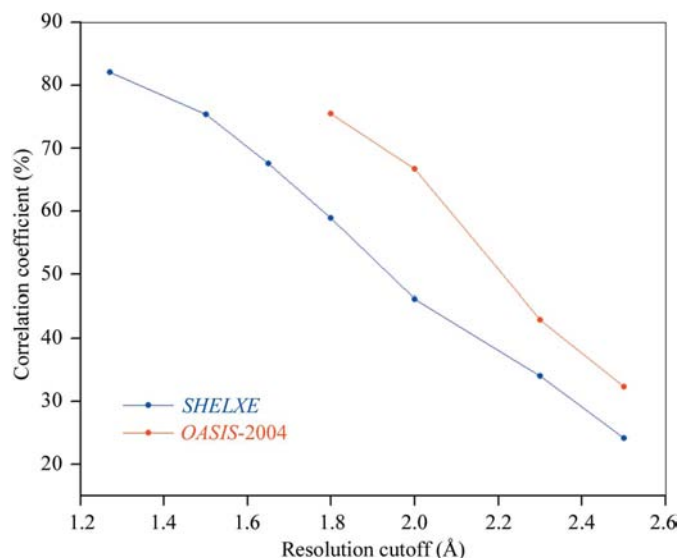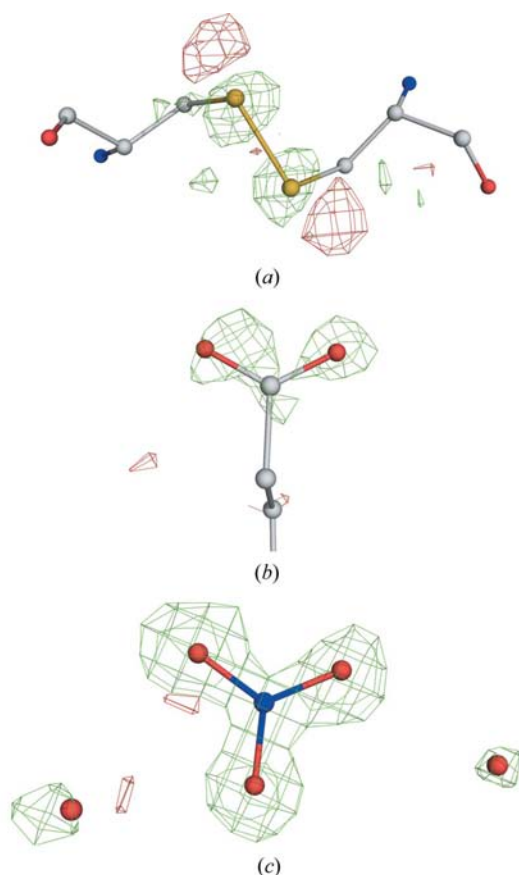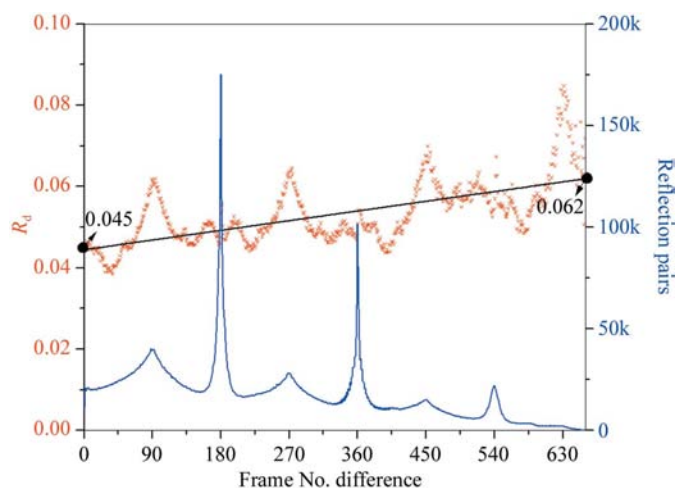

Figure 6
Iterative improvement of the electron-density map with increasing number of anomalous atoms located and used for phasing with data set 120 by *SHELXE*; three sites were located in cycle 1 (*a*), seven in cycle 2 (*b*) and all 11 sites in the last cycle (*c*).

Figure 7
Correlation coefficients between maps calculated with the final refined phases and those obtained by SAD phasing with data 330 truncated to various resolution cutoffs.

Figure 9
The R_d plot (Diederichs, 2006). Red crosses show the dependence of pairwise merging R values on the distance of the image numbers on which the reflections occur. The black least-squares line indicates that on average R_d increases from 4.5 to 6.2% during collection of all 660 images. The blue line shows the number of pairs of reflections contributing to each R_d value. Both curves are strongly modulated every 90° (and more weakly every 45°) owing to the fact that the crystal was rotated almost exactly around its fourfold axis during data collection.

Figure 8
Selected sites of radiation damage illustrated with the map calculated with final refined phases and differences of amplitudes merged from images 1–90 (first 45° of data) and images 570–660 (last 45° of data). (*a*) Disulfide bridge Cys178–Cys249; (*b*) carboxyl group of Glu43; (*c*) nitrate anion 501. The green contour is plotted at the map level of $+4\sigma$ in (*a*) and $+3.5\sigma$ in (*b*) and (*c*) and the red contours correspond to the analogous negative levels.

short wavelength of around 1 Å can not only provide the experimental phasing information for structure determination, but also the high-resolution native data set for structure refinement. In this example, a short wavelength has been used to collect the very weak anomalous signal from a crystal of proteinase K. With only one data set, the partial structure of anomalously scattering sites and experimental phases could be obtained from the anomalous signal, despite the presence of an identifiable radiation-damage effect suffered by the crystal. At the same time, the same 1.27 Å resolution data set was used to refine the structure to an R factor of 12.5%. If some compromises are made between the data multiplicity and the total exposure during diffraction experiments, an accurate beamline and good-quality crystal can provide an opportunity for the successful use of the very weak anomalous signal present in the data collected at short wavelength.

Coordinates and diffraction data (with Friedels unmerged) have been deposited in the PDB under entry 2id8.

References

Beardon, J. A. & Burr, A. F. (1967). *Rev. Mod. Phys.* **39**, 125–142.

Betzel, C., Gourinath, S., Kumar, P., Kaur, P., Perbandt, M., Eschenburg, S. & Singh, T. P. (2001). *Biochemistry*, **40**, 3080–3088.

Blundell, T. L. & Johnson, L. N. (1976). *Protein Crystallography*. New York: Academic Press.

Collaborative Computational Project, Number 4 (1994). *Acta Cryst.* **D50**, 760–763.

Dauter, Z. (1999). *Acta Cryst.* **D55**, 1703–1717.

Dauter, Z. (2006). *Acta Cryst.* **D62**, 867–876.

Dauter, Z., Dauter, M. & Dodson, E. (2002). *Acta Cryst.* **D58**, 494–506.

Dauter, Z., Dauter, M. & Rajashankar, K. R. (2000). *Acta Cryst.* **D56**, 232–237.

DeLano, W. L. (2002). *The PyMOL Molecular Graphics System*. DeLano Scientific, San Carlos, CA, USA.

Diederichs, K. (2006). *Acta Cryst.* **D62**, 96–101.

Emsley, P. & Cowtan, K. (2004). *Acta Cryst.* **D60**, 2126–2132.

Henderson, R. (1990). *Proc. R. Soc. London Ser. B*, **241**, 6–8.

Hendrickson, W. A. (1999). *J. Synchrotron Rad.* **6**, 845–851.

Hendrickson, W. A., Horton, J. R. & LeMaster, D. M. (1990). *EMBO J.* **9**, 1665–1672.

Hendrickson, W. A. & Ogata, C. M. (1997). *Methods Enzymol.* **276**, 494–523.

Hendrickson, W. A. & Teeter, M. M. (1981). *Nature (London)*, **290**, 107–113.

Howell, P. L. & Smith, G. D. (1992). *J. Appl. Cryst.* **25**, 81–86.

Kitago, Y., Watanabe, N. & Tanaka, I. (2005). *Acta Cryst.* **D61**, 1013–1021.

Minor, W., Cymborowski, M., Otwinowski, Z. & Chruszcz, M. (2006). *Acta Cryst.* **D62**, 859–866.

Mueller-Dieckmann, C., Panjikar, S., Tucker, P. A. & Weiss, M. S. (2005). *Acta Cryst.* **D61**, 1263–1272.

Murray, J. W., Garman, E. F. & Ravelli, R. B. G. (2004). *J. Appl. Cryst.* **37**, 513–522.

Olczak, A., Cianci, M., Hao, Q., Rizkallah, R., Raftery, J. & Helliwell, J. (2003). *Acta Cryst.* **A59**, 327–334.

Otwinowski, Z. & Minor, W. (1997). *Methods Enzymol.* **276**, 307–326.

Perrakis, A., Morris, R. & Lamzin, V. S. (1999). *Nature Struct. Biol.* **6**, 458–463.

Ramagopal, U. A., Dauter, M. & Dauter, Z. (2003). *Acta Cryst.* **D59**, 1020–1027.

Schneider, T. R. & Sheldrick, G. M. (2002). *Acta Cryst.* **D58**, 1772–1779.

Sheldrick, G. M. (2001). *XPREP*, v.6.14. Bruker–Nonius Inc., Madison, Wisconsin, USA.

Sheldrick, G. M. (2002). *Z. Kristallogr.* **217**, 644–650.

Sheldrick, G. M. & Schneider, T. R. (1997). *Methods Enzymol.* **277**, 319–343.

Terwilliger, T. C. (2003a). *Acta Cryst.* **D59**, 38–44.

Terwilliger, T. C. (2003b). *Acta Cryst.* **D59**, 45–49.

Wang, B.-C. (1985). *Methods Enzymol.* **115**, 90–112.

Wang, J.-W., Chen, J.-R., Gu, Y.-X., Zheng, C.-D. & Fan, H.-F. (2004). *Acta Cryst.* **D60**, 1991–1996.

Watanabe, N. (2006). *Acta Cryst.* **D62**, 891–896.

Watanabe, N., Kitago, Y., Tanaka, I., Wang, J., Gu, Y., Zheng, C. & Fan, H. (2005). *Acta Cryst.* **D61**, 1533–1540.

Xu, H., Yang, C., Chen, L., Kataeva, I. A., Tempel, W., Lee, D., Habel, J. E., Nguyen, D., Pflugrath, J. W., Ferrara, J. D., Arendall, W. B., Richardson, J. S., Richardson, D. C., Liu, Z.-J., Newton, M. G., Rose, J. P. & Wang, B.-C. (2005). *Acta Cryst.* **D61**, 960–966.

Yang, C., Pflugrath, J. W., Courville, D. A., Stence, C. N. & Ferrara, J. D. (2003). *Acta Cryst.* **D59**, 1943–1957.

Zwart, P. H. (2005). *Acta Cryst.* **D61**, 1437–1448.